Impact of the 2018 Ambae eruption on the global stratospheric aerosol layer and climate

Corinna Kloss[1], Pasquale Sellitto[2], Bernard Legras[3], Jean-Paul Vernier[4,5], Fabrice Jégou[1], M. Venkat Ratnam[6], B. Suneel Kumar[7], B. Lakshmi Madhavan[6], Gwenaël Berthet[1]

[1]Laboratoire de Physique et Chimie de l'Environnement et de l'Espace, CNRS/Université d'Orléans, UMR 7328, Orléans, France
Laboratoire Interuniversitaire des Systèmes Atmosphériques
[2]Laboratoire Interuniversitaire des Systèmes Atmosphériques, UMR CNRS 7583, Université Paris-Est Créteil, Université de Paris, Institut Pierre Simon Laplace, Créteil, France
[3]Laboratoire de Météorologie Dynamique, UMR 8539, CNRS – École-PSL/Sorbonne Université/École Polytechnique, Paris, France
[4]Science Systems and Applications, Inc, Hampton, Virginia, USA
[5]NASA Langley Research Center, Hampton, Virginia, USA
[6]National Atmospheric Research Laboratory, Department of Space, Gadanki-517112, India
[7]National balloon facility, TIFR, Hyderabad, India

Key Points:

- Two stratospheric eruptions occurred at the Ambae volcano in 2018, in April and July.
- Various satellite data reveal a significant impact on the global stratosphere.
- A significant radiative forcing is found for the eruption of July 2018.

Corresponding author: Corinna Kloss, `corinna.kloss@cnrs-orleans.fr`

Abstract

During an extended volcanic unrest starting in 2017, two main moderate stratospheric eruptions occurred at the Ambae volcano (15°S and 167°E), Vanuatu, in April and July 2018. Observations from a geostationary orbit show that the April and July eruptions injected a volcanic plume into the lower stratosphere. While aerosol enhancements from the April eruption have only had an impact on the Southern Hemisphere, the plume from the July eruption was distributed within the lower branch of the Brewer-Dobson circulation to both hemispheres. Satellite, ground-based and in situ observations show that the background aerosol is enhanced throughout the year after the July eruption on a global scale. A volcanic-induced perturbation of the global stratospheric aerosol optical depth up to 0.012 is found, in the ultraviolet/visible spectral range. This perturbation is comparable to that of recent moderate stratospheric eruptions like from Kasatochi, Sarychev and Nabro. Top of the atmosphere radiative forcing values are estimated between -0.45 and -0.6 W/m^2 for this event, showing that the Ambae eruption had the strongest climatic impact of the year 2018. Thus, the Ambae eruption in 2018 has to be taken into account when studying the decadal lower stratospheric aerosol budget and in climate studies.

1 Introduction

Major volcanic eruptions and the subsequent injection of sulfur compounds into the stratosphere are episodic events and their occurrence is currently unpredictable. Sulphur-containing gaseous emissions from volcanoes, in particular sulphur dioxide (SO_2), are subsequently converted to secondary sulphate aerosols (e.g. Kremser et al., 2016). These particles have a large lifetime because of their small average size and for the very limited wet deposition sink in the stratosphere. Additionally, they are very reflective and therefore have a big potential of cooling the climate system by the scattering of shortwave radiation. Depending on the magnitude of an eruption and geographical position of the volcano, the possible increased aerosol load in the stratosphere can have a strong impact on the Earth's climate (e.g. Robock et al., 2007; Kremser et al., 2016). For example, the geographical extent of the impact of a major tropical volcanic eruption is usually larger than that of an eruption at higher latitudes. In this case, aerosols formed in the tropical lower stratosphere can be transported within the stratospheric large-scale circulation (the Brewer-Dobson circulation, BDC (Butchart, 2014)) to higher latitudes. Aerosols resulting from a single eruption can be widely distributed around the globe, causing a significant 'global cooling' of the Earth's climate. The meridional dispersion is closely related to the phase of the quasi-biennial oscillation (QBO) (Trepte & Hitchman, 1992; Punge et al., 2009). While an easterly shear leads to the confinement of aerosols and a stronger ascent over the equator, the westerly shear reduces the ascent and favors dispersion to mid-latitudes. Even without the occurrence of major (Pinatubo-sized, as defined in Robock et al. (2007)) eruptions, it is known that during the past two decades the stratospheric aerosol load was still dominated by smaller to medium sized volcanic eruptions (Solomon et al., 2011; Vernier et al., 2011; Ridley et al., 2014). Multiple moderate volcanic eruptions took place during that period, with stratospheric injection and stratospheric aerosol measured perturbation (Ridley et al., 2014). For example, during the Sarychev eruption (48°N and 153°E on June 12th 2009) 1.2 ± 0.2 Tg of SO_2 were injected into the upper troposphere and lower stratosphere (UTLS). The most recent examples for moderate volcanic eruptions are the eruptions of Raikoke (48°N and 153°E on June 22nd 2019) and Ulawun (5°S and 151°E on June 26th 2019), injecting sulfate material at 17 km (Marder, 2019) and 19.2 km (Allon, 2019), respectively, into the stratosphere. Here, we study the impact of the Ambae (Vanuatu, 15°S and 167°E) eruptions of April and July 2018, on the global UTLS aerosol load and radiative balance. A special focus is given to the larger eruption of July 2018. To our knowledge, even though the eruptions (especially the one in July) were quite intense, their impact on the atmosphere and the climate system have not been investigated yet.

The paper is structured as follows. Methods and data sets used in the present study are described in Section 2. Recent activities and the major 2018 eruptions at Ambae are described in Section 3. The stratospheric aerosol evolution during the year following the eruptions is analyzed in Section 4, including in situ observations of the plume. The climate impact of this stratospheric aerosol perturbation is estimated and discussed in Section 5. Conclusions are drawn in Section 6.

2 Methods

2.1 OMPS-LP aerosol extinction satellite data set

The Ozone Mapping Profiler Suite Limb Profiler (OMPS-LP), onboard the Suomi National Polar-orbiting Partnership satellite, is a limb instrument part of a limb-nadir suite, initially developed for the three-dimensional monitoring of atmospheric ozone (Loughman et al., 2018; Bhartia & Torres, 2019). Cloud-filtered aerosol extinction profile measurements at 675 nm are provided from 2012 to now, in the 0-80 km altitude range, with a vertical resolution of ∼1.6 km (Bhartia & Torres, 2019). A global coverage is produced within 3-4 days. Here, we use the data version 1.5 (Chen et al., 2018). Tropopause values are provided by the MERRA-2 forward processing.

2.2 SAGE III/ISS aerosol extinction satellite data set

The Stratospheric Aerosol and Gas Experiment on the International Space Station (SAGE III/ISS) is a solar (and lunar) occultation measurement instrument onboard the International Space Station (ISS). We use the aerosol extinction data set version 5.1 at different wavelengths (384, 449, 521, 676, 756, 869, 1020 nm). Data are available from June 2017 onwards, with about 30 measurement profiles per day, between 60°S and 60°N. Aerosol extinction profile values are given on a vertical 0.5 km grid, between 0.5 and 40 km altitude with a vertical resolution of ∼1 km. Along the line of sight between the instrument and the sun, the horizontal resolution is ∼200 km, which is additionally extended by ∼200 km along the direction of motion of the ISS. We are focusing on altitudes above the tropopause. The tropopause information is derived from MERRA-2 (Modern-Era Retrospective analysis for Research and Applications, Version 2) reanalysis. For the single profiles used in this study, no cloud filter was applied. For the supplementary material (Fig. S3), a simple cloud filter has been applied as described in Thomason and Vernier (2013).

2.3 Himawari brightness temperature

Himawari-8, developped by the Japanese Space Agency, is a geostationary satellite, stationed at 140°E, to cover East Asia and the Western Pacific region (Da, 2015). It is equiped with a 16-channels multispectral imager, operating in the visible and infrared spectral regions. The spatial resolution at sub-satellite point is 0.5 to 1 km, for the visible, and 2 km, for the infrared channels. In this study, we make use of the infrared brightness temperature (BT) 6-hourly observations (Uesawa, 2009), which is part of the CSR (Clear Sky Radiance) product.

2.4 CALIOP

The Cloud-Aerosol Lidar with Orthogonal Polarization (CALIOP) onboard the CALIPSO satellite is a nadir-viewing active LiDAR sounder, operating since 2006. It measures the elastic backscatter at 532 nm and 1064 nm and the depolarization at 532 nm (Winker et al., 2010). It has a vertical resolution of 60 m below 20.3 km altitude and 180 m in the stratosphere (Winker et al., 2006). For the analysis in this study, a filter was applied, by removing pixels in the profile for which an adjacent pixel is cloudy.

2.5 LiDAR aerosol backscatter observations

An elastic backscatter ground-based LiDAR instrument is operational since 1998 at a rural location in Gadanki (13.5°N, 79.2°E) to study the properties of aerosols and cirrus clouds in the UTLS (SunilKumar et al., 2003; Kulkarni et al., 2008). This LiDAR system is a monostatic biaxial system and is optically aligned to altitudes greater than 8 km so that low-level clouds and aerosols do not interfer with the observations. Furthermore, the LiDAR is only operated during cloud-free (or clear sky) conditions. A total of 9 operational days were available from the LiDAR observational data set at Gadanki during January – February 2019 and are analysed in this study. Possible day-to day variabilities can result from the choice of a reference (calibration) altitude.

2.6 POPS in situ observations during the BATAL campaign

The Printed Optical Particle Spectrometer (POPS) was operated during the BATAL (The Balloon Measurements of the Asian Tropopause Aerosol Layer) campaign in 2019 in Hyderabad (17°N,78°E), India. The primary goal of this campaign is the investigation of the ATAL (Asian Tropopause Aerosol Layer) (Vernier et al., 2018). Here, we use POPS observations from one balloon flight on July 17^{th} 2019. The instrument weighs around 800 g and uses a 405 mm diode laser. POPS delivers aerosol number concentration and size distribution measurements in the size range 140-3000 nm (Gao et al., 2016). In this work, we make use of the cumulative concentration (cm^{-3}) for particle sizes from 0.15-0.18 μm.

2.7 Radiative transfer modelling: UVSPEC radiative forcing

The daily-average regional shortwave surface and top of the atmosphere (TOA) direct radiative impacts are estimated using the UVSPEC (UltraViolet SPECtrum) radiative transfer model, as implemented within the LibRadtran Mayer and Kylling (2005) package (available at: http://www.libradtran.org/doku.php). Surface and TOA direct and diffuse shortwave spectra are computed in the range 300 to 3000 nm, at 0.1 nm spectral resolution. The solar flux spectra of Kurucz are used to force the simulations. The atmospheric state (vertical profiles of temperature, pressure, humidity and gas concentration) is set using the AFGL (Air Force Geophysics Laboratory) climatological standards for: 1) a summer mid-latitude atmosphere for simulations representing the average southern and northern hemispheric dispersion of the Ambae plume, and 2) a tropical atmosphere for the simulation representing the average early tropical dispersion following the initial Ambae stratospheric injection. Molecular absorption is parameterized with the LOWTRAN band model, as adopted from the SBDART code. The SDISORT method (the pseudo-spherical approximation of the discrete ordinate method (DISORT)) is then used to solve the radiative transfer equation. We perform clear-sky simulations. A baseline simulation is carried out, with the mentioned setups and a background atmosphere without volcanic aerosols. Then, we add the measured volcanic aerosols spectral extinction coefficient profiles from SAGE III/ISS. The altitude ranges affected by the Ambae plume have been identified using the vertical profiles of the Angström exponent, as described in Sect. 5. In a similar manner as in Sellitto et al. (2016) and Kloss et al. (2019), for both the baseline and volcanic plumes configurations, we multiple-run the radiative transfer simulations at different solar zenith angles (SZA). Then, the daily-average shortwave TOA radiative forcing for the volcanic aerosol layer is calculated as the SZA-averaged upward diffuse irradiance for a baseline simulation without the investigated aerosols minus that with aerosols, integrated over the whole shortwave spectral range. Analogously, the shortwave surface radiative forcing is calculated as the SZA-averaged downward global (direct plus diffuse) irradiance with aerosols minus the baseline, integrated over the whole spectral range.

3 The Ambae volcanic unrest in 2017-2018 and the eruptions of April and July 2018

The Ambae or Aoba volcanic island (167°E and 15°S) is part of the Vanuatu archipelago, and located in its central sector. The explosive volcanic activity of Ambae results from the subduction of the Australian plate underneath the Pacific plate (Daniel et al., 1989). Its summit volcano reaches an altitude of almost 1500 m above sea level and includes 3 acid crater lakes. The volcano poses a significant volcanic hazard to the 11000 local inhabitants of the island (Bani et al., 2009). After an estimated 350-year volcanic quiescence (except for fumarolic and other hydrogeologic manifestation of its internal activity), a low-level activity resumed during the 1990s, followed by a strong eruptive phase starting from September 2017 (Moussallam et al., 2019). In 2018, a first paroxysm occurred on April 5^{th} around 14 UTC, when a SO_2-rich eruption occurred with an estimated sulfur load of 0.10-0.15 Tg of SO_2 (Carn, 2018). Himawari observations show a plume with a core brightness temperature (BT) of 193 K, for this event (Fig. S1a). Co-located temperature profiles from ERA5 reanalyses (Fig. S1b) indicate that this temperature corresponds to an altitude of about 17 km, which is taken here as a lower bound of the injection altitude. The actual injection altitude might be higher as the volcanic plume top is often colder than the ambient air (Woods & Self, 1992). In April, this was still the largest stratospheric volcanic sulfur emission since 2015. In July, however, the activity increased and entered its peak phase (Moussallam et al., 2019). A peak in sulfur emissions was observed on July 27^{th} (Marder, 2019). During this peak eruptive phase, about 0.4 Tg of SO_2 was emitted into the UTLS (Marder, 2019). It hit the news as the largest eruption, in terms of atmospheric sulfur injection during 2018, emitting three times more SO_2 than all eruptions combined in 2017. The eruptive phase, even if declining in magnitude, lasted until September 2018. The maximum VEI (Volcanic Explosivity Index) was 3 during the peak activity (GVP, 2018). We set our focus on the July eruption, which is the strongest in terms of emission burden and injection altitude for the 2018 active Ambae eruption phase. In Fig. 1 we show Himawari hourly BT in the 10.4 μm window around the Ambae volcano location on July 27^{th}, 2018. The cold plume is apparent starting from 01:00, developing in the following hours with a fairly clear sky environment and dispersing eastwards due to the dominant UTLS westerly winds until it is unrecognizable as it merges with clouds (Fig. 1a). Fig. 1a likely shows the initial ash injection and/or condensed volcanic water clouds in this phase. In Fig. 1b, an enlarged view of the initial plume at 02:00 of July 27^{th} is given, showing that the lowest BT at the core of the plume is around 205 K. Co-located ERA5 temperature profiles show that this temperature is found around the tropopause and lower-stratosphere, either at 14 or 18 km altitude. We thus conclude that this injection was at least partly stratospheric. Observations of SO_2 plume altitude with IASI (Infrared Atmospheric Sounding Interferometer) confirm a plume injection above 15 km, for this event (Aeris, 2018). Unfortunately, there were no conveniently located orbits of CALIPSO that day.

4 Ambae aerosol plume dispersion in the global lower stratosphere

To study the horizontal, global distribution of the enhanced aerosol layer in the lower stratosphere, an overview of OMPS-LP aerosol extinction observations, over the course of one year after the main eruption in July 2018, is shown in Fig. 2. For the first sulfur rich eruption from Ambae on April 5^{th} 2018, we see a residual aerosol extinction enhancement in the lower stratosphere (up to 18 to 19 km altitude) 30° in longitude further west of the Ambae location (Fig. 2a). The volcanic plume was likely transported westwards at around 17-18 km altitude.

For the more intense Ambae eruption on July 27^{th}, a first aerosol extinction enhancement at 19-20 km altitude (∼1 km higher than the previous Ambae eruption) is observed around 10° further east at latitudes consistent with the Ambae location (15°S) in the end of July (Fig. 2b). One month later the plume was distributed in both direc-

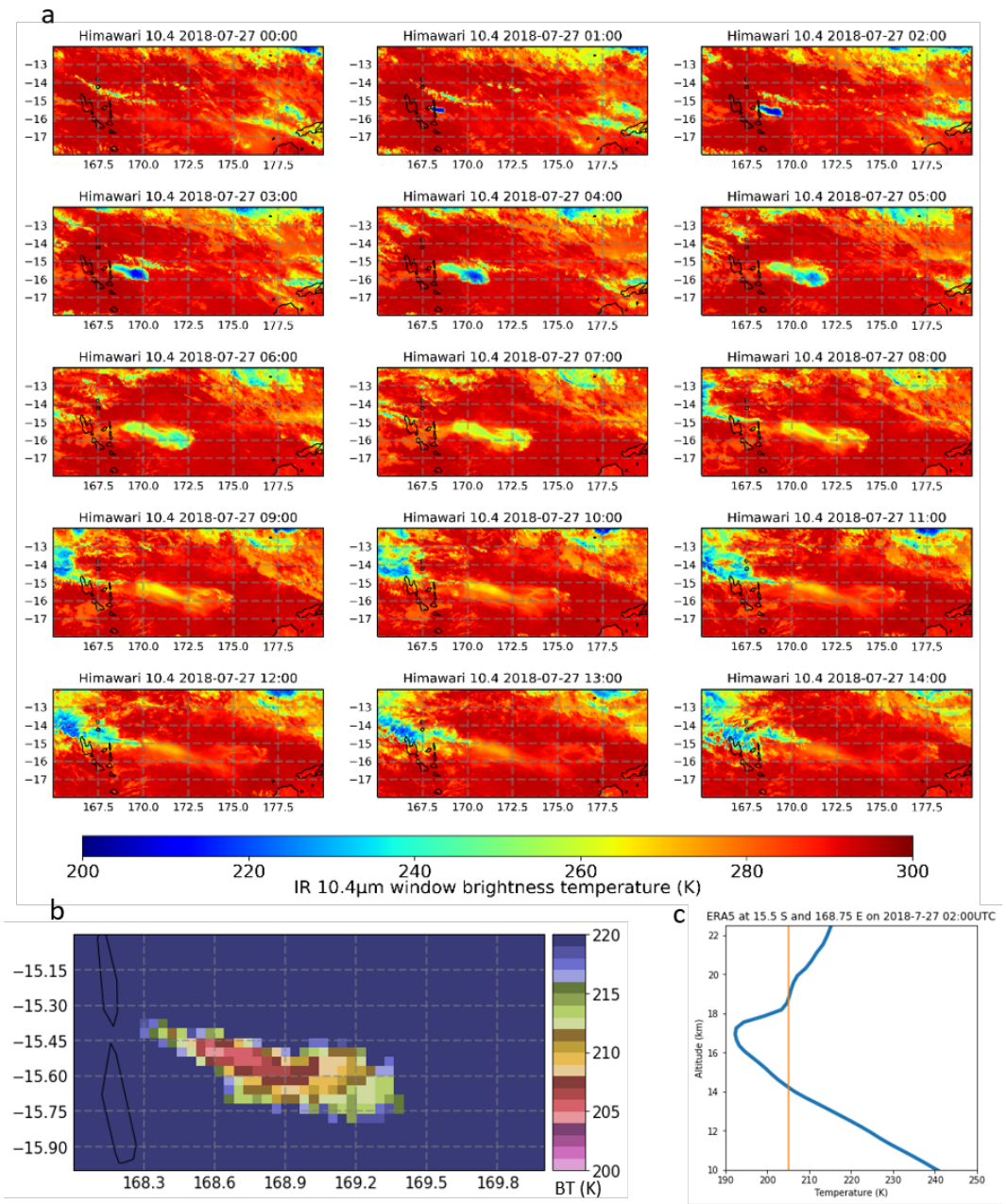

Figure 1. (a) Himawari infrared brightness temperature (BT) hourly observations around Ambae volcano location (black triangle in the upper-left panel) on July 27^{th}, 2018, from 00:00 (upper-left panel) to 14:00 LT (lower-right panel). All times are indicated in local time, LT. (b) Zoomed-in BT, with enhanced color scale, around Ambae for July 27^{th}, 02:00. (c) ERA5 temperature profile at the location of the minimum BT of Fig. 1b (blue line) and a reference vertical line (yellow line) for 205 K.

tions east and west (Fig. 2c). With the dominating eastward transport, the plume propagated fast over the Pacific. The westward propagation over the Indian Ocean has been quite slow and the plume has stayed a long time over New Guinea. Within two months (by the end of September, Fig. 2d), the tropics in the SH, but also a part of the NH tropics, are filled with a dense enhanced aerosol layer. Fig. 3 shows CALIOP vertical profile observations and the latitudinal distribution of aerosols, at this stage of the dispersion of the plume (in early September). A dense, vertical localized, aerosol layer between about 17 and 21 km is observed, between around 15°S and 5°N. Vertical and horizontal CALIOP distributions of the Ambae volcanic aerosol plume at the end of September are shown in Fig. S2. At this time, most of the global tropics, especially in the SH, are affected by this UTLS plume. At these altitudes, a typical expected time scale of sulphates formation from SO_2 emissions is some weeks to a few months (e.g. Stevenson et al., 2003), which is consistent with OMPS-LP observations. From there, the newly formed aerosol layer is slowly distributed to higher latitudes, in both hemispheres, within the shallow branches of the BDC (Nov 2018-Feb 2019, Fig. 2e-g). Even though the eruption occurred in the SH, by February 2019 (Fig. 2g) the largest part of the enhanced aerosol signature at 19-20 km altitude is observed in the NH. This can be linked to the occurring phase of the QBO and the seasonal cycle. During summer 2018 the QBO was in its easterly phase in the lower stratosphere Newman et al. (2019). According to Trepte and Hitchman (1992) when the easterly shear is present, confinement within the tropical band is favored with respect to the dispersion to the mid-latitudes. Nevertheless, there is a seasonal displacement to the winter hemisphere during solstitial season (Punge et al., 2009) which on the contrary favors dispersion. Hence, the mid-latitude dispersion occurs mostly in the NH.

Six months after the eruption (Dec 2018, in Fig. 2f), when the tropical UTLS is filled with volcanic aerosol from Ambae, aerosol extinction values are in average increased by 80% at 19-20 km altitude compared to the conditions prior to the eruption. In July 2019 (one year after the Ambae eruption, Fig. 2i) the mean aerosol extinction at 19-20 km is still enhanced by around 50%, however it cannot be excluded that other volcanic eruptions (e.g. Raikoke and Ulawun) and wildfires can have contributed at that point to the background aerosol. The enhanced aerosol extinction areas above south America (at 0-10°S and 50-130°W) in Fig. 2i might be linked to the Ulawun eruption, which occurred at 5°S and 151°E on June 27^{th} 2019 and was then (as the Ambae plume) transported to the East.

In-situ POPS aerosol concentration and LiDAR backscatter measurements coupled with the mean OMPS aerosol extinction data for the red area in Fig. 2 confirm the temporal evolution of the Ambae plume and add vertical information for the main event of July 2018 (Fig. 4). LiDAR observations (Fig. 4a) show an increase in the aerosol backscatter signal at altitudes from 18 to 22 km for all available profiles in January and February 2019. Fig. 4b shows enhanced aerosol concentration values in mid-July 2019 from balloon-borne in situ measurements on altitudes between ∼16 and 24 km altitude. The POPS measurements are representative for particle sizes from 0.15 to 0.18 μm. These aerosol enhancements are consistent with co-localized observed OMPS vertical profiles (Fig. 4c). This agreement helps tracing back the stratospheric aerosol enhancements in POPS and LiDAR measurements to the Ambae eruption in July 2018. Vertical-localized enhancements in Fig. 4b, below 20 km altitude can point to the presence of enhanced aerosol in the Asian monsoon anticyclone (i.e. the ATAL: Asian Tropopause Aerosol Layer, Fadnavis et al. (2013), Vernier et al. (2015)). Based on OMPS observations in Fig. 4c, an enhanced aerosol layer reaches the red area already in October 2018 in the lower stratosphere at altitudes of around 18 km. The main bulk of the enhanced aerosol layer arrives in December 2018 at around 20 ± 2 km. In October and November 2018, the aerosol layer reaches the respective area on different altitudes, equivalent to an uplifting feature of ∼0.6 mm/sec (3 km within 2 months). The velocity calculation is based on aerosol extinction values between 4 and 6 10^{-3} km^{-1}. This is in good agreement with the tropical upwelling velocity as analyzed in Abalos et al. (2015) and is very similar to what has

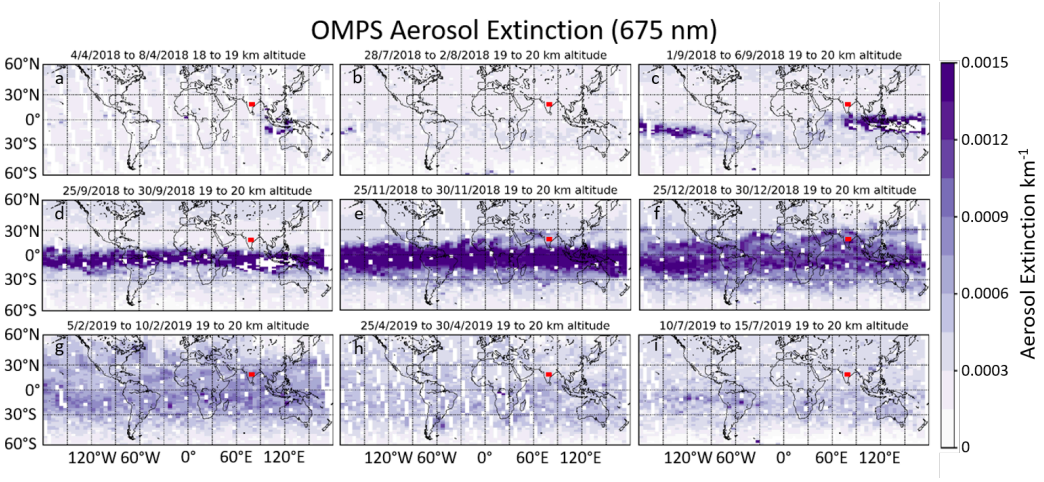

Figure 2. OMPS Aerosol extinction distribution between 19 and 20 km (18-19 for a) altitude from summer 2018 to summer 2019 at 675 nm. Extinction values are averaged over the respective time frames. The red box indicates the position of the BATAL campaign 2019 (see BATAL observations in Fig. 4a).

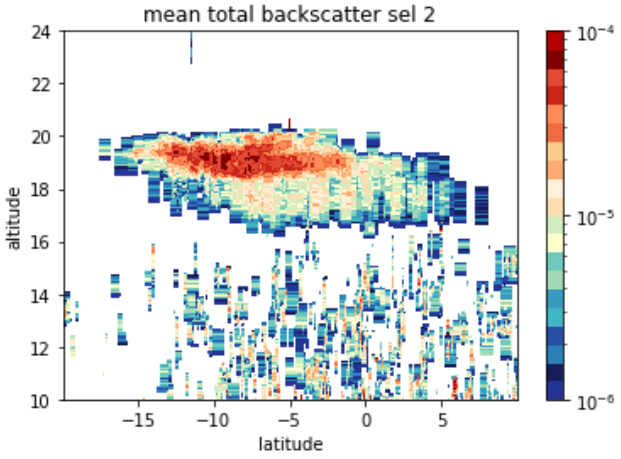

Figure 3. CALIOP mean total backscatter profiles and a function of the latitude, in the extended Indian Ocean (longitude interval: 0-150°E), during early September (September 1^{st} to 15^{th}). This figure was obtained by averaging the level 2 CALIOP aerosol profile product over 63 night orbits crossing the domain during the time interval.

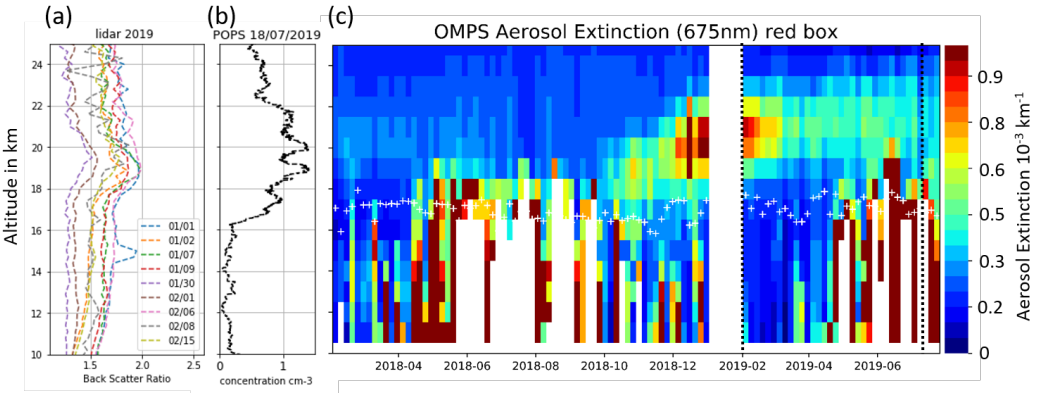

Figure 4. (a) Effective backscatter ratio LiDAR measurements in January and February 2019 at Gedanki (13.5°N and 79.2°E).(b) In situ POPS aerosol concentration measurements at 17.5°N and 78.2°E, observed during the BATAL campaign in 18/07/2019 for particle sizes from 0.15 to 0.18μm. (c) OMPS aerosol extinction measurements (at 675 nm) averaged over 17-21°N,76-82°E (location indicated with a small red area in Fig. 2) with 5-days averages. The point in time of the in situ profiles from (a) and (b) are indicated with the black dotted lines. White plus signs represent the mean tropopause altitude for the averaged profiles.

been observed for aged forest fire aerosols for a similar area (0.64 mm/sec in Kloss et al. (2019)). No diabatic, radiative-based self-lifting of the plume is expected for this event, due to the very likely non-absorbing aerosols in the plume (Ditas et al., 2018). Between December and June, the aerosol layer remains on the same altitude range. Similar conditions are observed on the same latitudes around the globe. The April eruption on Ambae is not expected to play a significant role for the enhancements observed in Fig. 4c.

Figure 5 shows the zonal mean distribution as a function of latitude (60°S to 60°N, at 26-32°W) in mid-February 2019. The longitude range is chosen to exclude enhancement of tropospheric aerosols due to regional sources. At this time, 5 months after the eruption, the tropics are filled with an enhanced aerosol signal at 19-20 km altitude (Fig. 2g) and the aerosol plume is already globally, largely distributed and dispersed. Enhanced aerosol air masses already start descending in the extra-tropics at latitudes $> 40°$. The observed transport of the Ambae aerosols towards higher latitudes and descent nicely follow the mid-latitude descending lower branch of the BDC in the winter hemisphere. Enhanced aerosol extinction values are still observed above around 15°S ($\pm 10°$), the latitude band of injection at around 21 km (± 2 km) altitude. This shows that while the plume has already efficiently been transported towards the north within the BDC, by February large air masses have still remained at injection latitudes. The observed descent within the lower branch of the BDC of 10 km within 3 months (1.3 mm/s) matches well the values given in Abalos et al. (2015). Fig. 5 shows a more substantial distribution towards the NH for the chosen time, suggesting a more efficient transport towards the north (as also suggested in Fig. 2).

Figure 6 presents the time series of the mean aerosol extinction at two altitude levels respective to the tropopause altitude (1 to 2 km and 3 to 4 km above the tropopause) for four latitude bands (representative for the tropics, the mid-latitudes in the SH and NH and northern high latitudes), from April 2017 to August 2019. The extended time interval prior to the Ambae eruptions displays the 'background' conditions. A non-volcanic event, the wildfires in British Columbia in mid-August 2017 that induced strong pyro-convection, shows up as a sudden smoke particle enhancement in the lower stratosphere (Khaykin et al., 2018). A distinguished transport pathway of this fire plume to the tropical lower stratosphere via the circulation of the Asian monsoon anticyclone is demon-

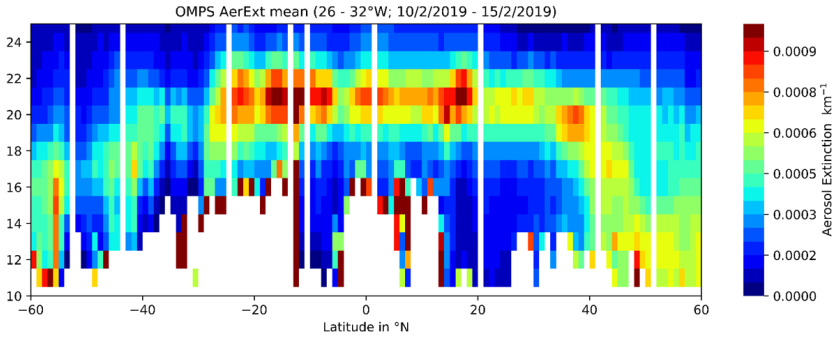

Figure 5. OMPS aerosol extinction data (at 675 nm) averaged for each 1° latitude bin between Feb 10-15th at 26-32°W.

strated in Kloss et al. (2019). Due to the large area averaged in Fig. 6, the impact of those smoke particles on the tropical lower stratosphere is hardly identified here. However, Fig. 6 suggests that the lower stratosphere at 30-90°N was still impacted by the 2017 Canadian fires in the end of June 2018, about two months longer than suggested by Yu et al. (2019).

From the end of April to the end of June 2018, Fig. 6 shows enhanced aerosol extinction values in the mid-latitudes in the SH (30-50°S, blue line), that we attribute to the first intense Ambae eruption of April 2018. The increase in aerosol extinction is visible within both chosen altitude ranges (1-2 and 3-4 km above the tropopause, blue line in Fig. 6). Furthermore, a slightly enhancement of the background aerosol in the tropics at 1-2 km above the tropopause is visible (red line, April-July 2018 in Fig. 6b). The peak in aerosol extinction values in the tropics and SH, starting end of July 2018 at both altitude ranges shown in Fig. 6, is due to the stronger July eruption at Ambae. The aerosol enhancement reaches a maximum in the beginning of October 2018 with almost four times higher mixing ratios than prior to the main eruptive phase of Ambae. In the tropics and SH mean mixing ratios decrease and are back to 'normal' (i.e. prior to Ambae 2018 eruptions) 1-2 km above the tropopause, within 9 months (by March 2019). At higher altitudes (3-4 km above the tropopause in Fig. 6a) the decrease is lower and especially in the tropics, aerosol extinction values still double 'background conditions' in June 2019. The mean mixing ratios at northern higher latitudes increase and remain enhanced for more than 11 months, until July 2019 (1-2 km above the tropopause, Fig. 6b). This can be explained by the transport of plume air masses from the lower stratosphere in the tropics towards the poles within the BDC. While the July eruption shows a global impact on the lower stratosphere (i.e. increasing signatures in the tropics, SH and NH), only the SH seems to be impacted for the April eruption. Two factors play a role in explaining why the second eruption in July 2018 shows a globally bigger influence than the eruption in April 2018: 1st the sulfur emissions of the July eruption is by a factor of ∼4 larger and 2nd the injection altitude in April was lower (by at least 1 km, this is also confirmed by Fig. 6) and therefore the chances of a long-range transport within the BDC are lower.

The enhanced aerosol extinction values in the NH have not yet decreased back to 'prior'-Ambae conditions, when two new volcanic eruptions occurred at the right end of the time interval displayed in Fig. 6. The increase in aerosol extinction values in the tropics and, in particular the SH, 1-2 km above the tropopause is associated with the Ulawun eruption (Papua New Guinea, June 2019). The distinct enhancement in the NH is associated with the strong Raikoke eruption (Russia, June 2019). The direct and fast injection of ashes followed by a decay is different from the Ambae case, for which the slow increase from end of July to the beginning of October 2018 (as well as from the beginning of April to the beginning of May 2018, for the April eruption) rather points to the

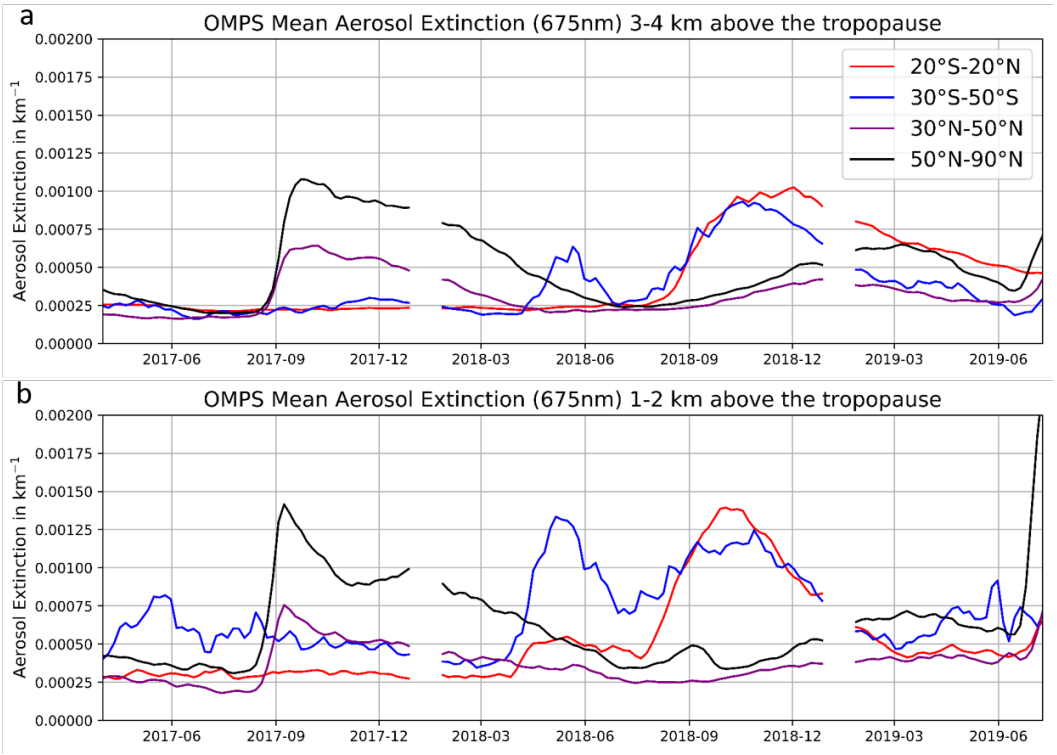

Figure 6. Mean aerosol extinction values 3-4 km and 1-2 km above the tropopause in the tropics (20°S-20°N: blue), in the mid-latitudes (30-50°S and 30-50°N) and in the North (50-90°N).

in situ production of secondary aerosol. A direct injection of ash particles would result in a sudden aerosol increase, as it is observed for the Raikoke eruption. At its latitude (48°N), the tropopause is low and a direct injection of ash particles into the UTLS is very likely to happen, even from a moderate volcanic eruption. Other primary aerosol injections, like fire aerosols from the Canadian wildfire in summer 2017, produce a similar steep temporal signature followed by a decay (also visible in Fig. 6)

5 Optical properties of the volcanic plume and the global impact on the radiative balance

The Ambae plume evolution has also been observed with SAGE III/ISS. This instrument, though providing sparser observations with respect to OMPS-LS due to its solar occultation geometry, has a better signal-to-noise ratio. In addition, spectrally-resolved observations are provided, i.e. at 7 different wavelengths between 380 and 1020 nm. This allows a further characterization of the plume's optical properties. The spatial dispersion of the plume (Fig. S3a), and its vertical (Fig. S3b) and latitudinal evolution (Fig. S3c) are very similar to OMPS-LP observations discussed in Sect. 4. Based on this agreement, we use SAGE III/ISS data to study the spectral dependency of the plume's extinction. Fig. 7a shows the aerosol optical depth (AOD) for the averaged plume observations from SAGE III/ISS in three latitude bands: the tropics (20°S-20°N), the NH (50-90°N) and the SH (30-60°S), as also chosen in Fig. 6. The latitude band in the NH 50-60°N, rather than 50-90°N is due to the fact that SAGE III/ISS does not perform measurements poleward of 60°. Different time intervals are chosen based on the picture drawn

by OMPS-LP observations of Fig. 6, to represent the plume dispersion and the characteristic perturbation of the Ambae plume in the three latitude bands: from September 28^{th} 2018 to October 19^{th} 2018 in the tropics, from March 1^{st} 2019 to April 15^{th} 2019 in the NH and from September 9^{th} 2018 to November 4^{th} 2018 in the SH. The plume has been identified, in the average SAGE III/ISS vertical profiles, using a criterion based on the vertical variability of the computed Angström exponent (AE), using the aerosol extinction values at 449 and 869 nm. The AE is an optical proxy for average size particles; bigger AEs point to the presence of smaller particles and vice-versa (van de Hulst, 1981). Large values of the AE (e.g. larger than 1.5) and aerosol extinction can be linked to small sulphate aerosol (e.g. Sellitto et al., 2016, 2017). Altitudes impacted by the volcanic plume are chosen where vertically-isolated regions with larger aerosol extinction (linked to an aerosol perturbation from the background conditions) and large AE (linked to smaller particles than background conditions) are simultaneously found. For the three averaged profiles, in the tropics, NH and SH, abrupt variations of the AE (larger values, generally >1.5, than at lower or higher altitudes) are found (Fig. 8), which are co-localized with unusual peaks in the aerosol extinction profile. This is a strong indication that these altitudes are linked to the Ambae plume. In the present case, aerosol extinction perturbations, possibly linked to small sulphate aerosols, result from the conversion of SO_2 emissions of Ambae. Based on this, we find the vertical regions affected by the Ambae plume: from 16.5 to 21.5 km in the tropics, from 13 to 21 km in the NH and from 12.5 to 20 km in the SH. The averaged AE at these altitudes are 1.7, 1.8 and 2, respectively. During the dispersion, from the tropics to the SH and NH, the AE value increases, indicating further formation of small sulphate particles with time. From this definition of the latitudinal/vertical-dependent perturbation of the Ambae plume, the plume-isolated average AOD at different wavelengths are derived for a selection of wavelengths (Fig. 7a). Typical AOD values of 0.008 to 0.012, in the near-infrared, and 0.006 to 0.008, in the visible, are found, which points to a sensible perturbation of the lower stratospheric aerosol extinction. This AOD perturbation is comparable, even if slightly smaller, to that of the recordbreaking Canadian wildfire of 2017 (Kloss et al., 2019). Larger AOD values are found in the SH at later time frames, which point to a progressive build-up of a secondary aerosol plume from SO_2. The volcanic AOD perturbation in the UTLS from Ambae is comparable, albeit slightly smaller, to other previous, recent moderate stratospheric volcanic eruptions, like the ones from Kasatochi, Sarychev and Nabro. The peak AOD perturbation at 532 nm of these three eruptions has been estimated at ∼0.012, 0.012 and 0.09 at the global scale, respectively (Andersson et al., 2015). It has to be noted that none of these three eruptions had a substantial impact on the SH UTLS aerosol distribution (Andersson et al., 2015). Ambae eruption is a peculiar event, from this point of view.

Furthermore, we calculated the shortwave radiative forcing (RF) of the Ambae UTLS plume using the UVSPEC radiative transfer model (the setup of the model is described in Sect. 2.7). As input parameters for the model, the SAGE III/ISS latitudinally-averaged and Ambae-attributed aerosol extinction profiles are used. Some assumptions are needed, regarding the optical properties of the plume. Based on the above discussion, we assume that the plume is dominated by strongly reflective and small sulphate particles. Hence, typical values of the single scattering albedo (SSA, 0.99) and the asymmetry parameter (g, 0.5) for these particles are chosen (Sellitto & Briole, 2015). As these optical parameters are not measured, we perturbed our RF calculations with smaller SSA (down to 0.98) and larger g (up to 0.7). These RF estimations are shown in Fig. 7b, for three latitude bands (30-50°S, 20°S-20°N and 50-60°N). The surface and TOA RF are very similar, which is typical for highly-reflective particles. Correspondingly, a very small amount of energy is released to the atmosphere by the interaction of solar radiation and the plume, as it is largely non-absorbing. However, globally relatively large negative TOA RF values are observed, with values spanning from about -0.45 to -0.60 W/m^2. This RF is comparable to the ones from Kasatochi, Sarychev and Nabro (e.g. Ridley et al., 2014; Andersson et al., 2015). For these three recent eruptions, RFs between -0.40 and -0.50 W/m^2

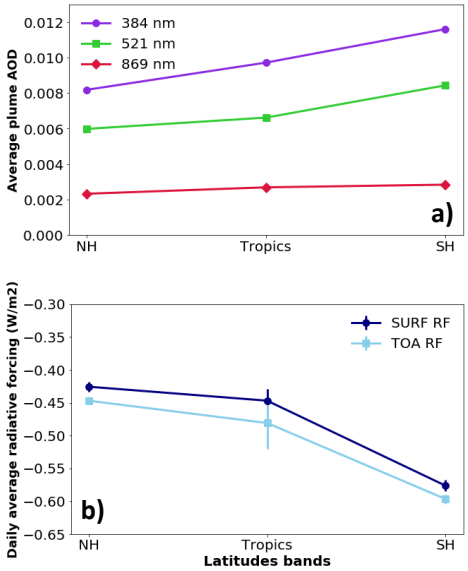

Figure 7. (a) Averaged plume Optical Depth (AOD) for the average SAGE III/ISS observations in the tropics (20°S-20°N: 28/09/2018-19/10/2018), in the Southern Hemisphere (30-50°S: 09/09/2018-04/11/2018) and in the Northern Hemisphere (50-90°N: 01/03/2019-15/04/2019). Time frames are chosen according to the increased aerosol extinction values as seen in Fig 6. (b) Daily average radiative forcing (W/m^2) for the surface (SURF) and Top of the atmosphere (TOA) for SAGE III/ISS mean aerosol extinction profiles as described in Fig. 6.

are found. Bigger values are found for Ambae when dispersing in the SH during austral spring and summer.

6 Conclusions

The volcanic events of Ambae in April and July 2018 injected substantial amounts of SO_2 into the tropical UTLS, where secondary aerosol particles were formed. The eruption of July 2018 produced a noticeable perturbation in the UTLS aerosol distribution on a global scale. With a dispersion in the lower stratosphere to the NH and SH within the lower branch of the BDC, it had a substantial impact on the global stratospheric aerosol extinction. It has previously been suggested that the Ambae eruption 2018 has had a very limited impact on the global climate (Marder, 2019). However, we have found a TOA radiative forcing of the same magnitude than previous widely studied moderate volcanic eruptions (e.g. Sarychev, Nabro). In addition, the Ambae aerosols were distributed into both hemispheres and persisted for several months in the global stratosphere with a significant radiative forcing. The impact of Ambae eruption on the stratospheric aerosol optical depth and radiative balance in the SH is peculiar. We conclude that the Ambae eruption should be considered in future analyses of the integrated climatic impact of moderate stratospheric volcanic perturbations.

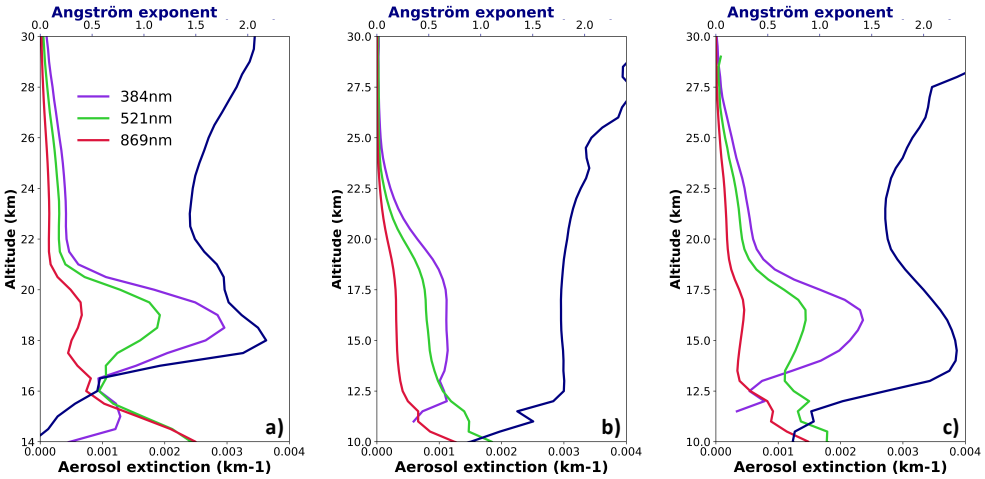

Figure 8. Averaged vertical profiles of SAGE III/ISS aerosol extinction at 384 (purple line), 521 (green line) and 869 nm (red line), and Angström exponent (blue line), for the tropics (a), NH (b) and SH (c). The profiles are average over Ambae-plume-impacted periods defined in the text.

Acknowledgments

The authors acknowledge the support of Agence Nationale de La Recherche under grant ANR-17-CE01-0015 (TTL-Xing). Corinna Kloss was funded by Deutsche Forschungsgemeinschaft (DFG, German Research Foundation) – 409585735. The providers of the LibRadtran are gratefully acknowledged. Furthermore, the authors acknowledge the National Aeronautics and Space Administration (NASA), the SAGE III/ISS and OMPS teams, as well as the BATAL campaign coordinators.

Data availability: The SAGE III/ISS aerosol extinction data set (version 5.1) is available at https://eosweb.larc.nasa.gov, the OMPS aerosol extinction data set (version 1.5) at https://daac.gsfc.nasa.gov/. Himawari and CALIOP data are provided by AERIS/ICARE data centre (https://en.aeris-data.fr/direct-access-icare/), the ERA5 data are available from Copernicus Climate Change Service (https://climate.copernicus.eu/climate-reanalysis). POPS and LiDAR measurements archiving on AERIS/ICARE data center is ongoing.

References

Abalos, M., Legras, B., Ploeger, F., & Randel, W. J. (2015). Evaluating the advective Brewer-Dobson circulation in three reanalyses for the period 1979–2012. *J Geophys Res*, *120*(15), 7534-7554. Retrieved from `https://agupubs.onlinelibrary.wiley.com/doi/abs/10.1002/2015JD023182` doi: 10.1002/2015JD023182

Aeris. (2018). *SO2 total column from IASI (Level 2).* Retrieved 2019-12-14, from `https://iasi.aeris-data.fr/so2/`

Allon, C. (2019). *Another High-Level Eruption Observed at Ulawun Volcano — Ash Column Rising to a Colossal 63,000 feet (19.2 km).* Retrieved 2019-12-08, from `https://electroverse.net/another-high-level-eruption-at-ulawun-volcano-ash-column-rising-to-63000-feet-19-2-km/`

Andersson, S., Martinsson, S., Vernier, J., Friberg, J., Brenninkmeijer, C., Hermann, M., ... Zahn, A. (2015). Significant radiative impact of volcanic aerosol in the lowermost stratosphere. *Nat Commun*, *7692*(6), 1–8. doi: doi:10.1038/ncomms8692

Bani, P., Join, J.-L., Cronin, S., Lardy, M., & Rouet, E. G. (2009). Characteristics of the summit lakes of Ambae volcano and their potential for generating lahars. *Natural Hazards and Earth System Sciences, European Geosciences Union*, *120*(4), 1471-1478. doi: 0.5194/nhess-9-1471-2009

Bhartia, P. K., & Torres, O. O. (2019). *OMPS-NPP L2 LP Aerosol Extinction Vertical Profile swath daily 3slit V1.5.* doi: 10.5067/GZJJYA7L0YW2

Butchart, N. (2014). The Brewer-Dobson circulation. *Reviews of Geophysics*, *52*(2), 157-184. Retrieved from `https://agupubs.onlinelibrary.wiley.com/doi/abs/10.1002/2013RG000448` doi: 10.1002/2013RG000448

Carn, S. (2018). Retrieved 2019-12-12, from `https://twitter.com/simoncarn/status/982272241546047494`

Chen, Z., Bhartia, P. K., Loughman, R., Colarco, P., & DeLand, M. (2018). Improvement of stratospheric aerosol extinction retrieval from OMPS/LP using a new aerosol model. *Atmos Meas Tech Discussions*, *2018*, 1–32. Retrieved from `https://www.atmos-meas-tech-discuss.net/amt-2018-221/` doi: 10.5194/amt-2018-221

Da, C. (2015). Preliminary assessment of the Advanced Himawari Imager (AHI) measurement onboard Himawari-8 geostationary satellite. *Remote Sensing Letters*, *6*(8), 637-646. Retrieved from `https://doi.org/10.1080/2150704X.2015.1066522` doi: 10.1080/2150704X.2015.1066522

Daniel, J., Gerard, M., Mauffret, A., Boulanger, D., Cantin, B., Collot, J.-Y., ... Tissot, J.-D. (1989). Déformation compres-sive d'un bassin intra-arc dans un contexte de collision ride/arc : le bassin d'Aoba, arc des Nouvelles-Hébrides. *CR Acad Sci II*, *308*, 239-245.

Ditas, J., Ma, N., Zhang, Y., Assmann, D., Neumaier, M., Riede, H., ... Cheng, Y. (2018). Strong impact of wildfires on the abundance and aging of black carbon in the lowermost stratosphere. *Proceedings of the National Academy of Sciences*, *115*(50), E11595–E11603. Retrieved from https://www.pnas.org/content/115/50/E11595 doi: 10.1073/pnas.1806868115

Fadnavis, S., Semeniuk, K., Pozzoli, L., Schultz, M. G., Ghude, S. D., Das, S., & Kakatkar, R. (2013). Transport of aerosols into the UTLS and their impact on the Asian monsoon region as seen in a global model simulation. *Atmospheric Chemistry and Physics*, *13*(17), 8771–8786. Retrieved from https://www.atmos-chem-phys.net/13/8771/2013/ doi: 10.5194/acp-13-8771-2013

Gao, R. S., Telg, H., McLaughlin, R. J., Ciciora, S. J., Watts, L. A., Richardson, M. S., ... Fahey, D. W. (2016). A light-weight, high-sensitivity particle spectrometer for PM2.5 aerosol measurements. *Aerosol Science and Technology*, *50*(1), 88-99. Retrieved from https://doi.org/10.1080/02786826.2015.1131809 doi: 10.1080/02786826.2015.1131809

GVP. (2018). *Ambae.* Retrieved 2019-12-14, from https://volcano.si.edu/volcano.cfm?vn=257030

Khaykin, S. M., Godin-Beekmann, S., Hauchecorne, A., Pelon, J., Ravetta, F., & Keckhut, P. (2018). Stratospheric Smoke With Unprecedentedly High Backscatter Observed by Lidars Above Southern France. *Geophysical Research Letters*, *45*(3), 1639-1646. Retrieved from https://agupubs.onlinelibrary.wiley.com/doi/abs/10.1002/2017GL076763 doi: 10.1002/2017GL076763

Kloss, C., Berthet, G., Sellitto, P., Ploeger, F., Bucci, S., Khaykin, S., ... Legras, B. (2019). Transport of the 2017 Canadian wildfire plume to the tropics via the Asian monsoon circulation. *Atmospheric Chemistry and Physics*, *19*(21), 13547–13567. Retrieved from https://www.atmos-chem-phys.net/19/13547/2019/ doi: 10.5194/acp-19-13547-2019

Kremser, S., Thomason, L. W., von Hobe, M., Hermann, M., Deshler, T., Timmreck, C., ... Meland, B. (2016). Stratospheric aerosol—Observations, processes, and impact on climate. *Reviews of Geophysics*, *54*(2), 278-335. Retrieved from https://agupubs.onlinelibrary.wiley.com/doi/abs/10.1002/2015RG000511 doi: 10.1002/2015RG000511

Kulkarni, P., Ramachandran, S., Bhavani Kumar, Y., Narayana Rao, D., & Krishnaiah, M. (2008). Features of upper troposphere and lower stratosphere aerosols observed by lidar over Gadanki, a tropical Indian station. *Journal of Geophysical Research: Atmospheres*, *113*(D17). Retrieved from https://agupubs.onlinelibrary.wiley.com/doi/abs/10.1029/2007JD009411 doi: 10.1029/2007JD009411

Loughman, R., Bhartia, P. K., Chen, Z., Xu, P., Nyaku, E., & Taha, G. (2018). The Ozone Mapping and Profiler Suite (OMPS) Limb Profiler (LP) Version 1 aerosol extinction retrieval algorithm: theoretical basis. *Atmos Meas Tech*, *11*(5), 2633–2651. Retrieved from https://www.atmos-meas-tech.net/11/2633/2018/ doi: 10.5194/amt-11-2633-2018

Marder, J. (2019). *2018's Biggest Volcanic Eruption of Sulfur Dioxide.* Retrieved 2019-12-07, from https://www.nasa.gov/feature/goddard/2019/2018-s-biggest-volcanic-eruption-of-sulfur-dioxide

Mayer, B., & Kylling, A. (2005). Technical note: The libRadtran software package for radiative transfer calculations - description and examples of use. *Atmospheric Chemistry and Physics*, *5*(7), 1855–1877. Retrieved from https://www.atmos-chem-phys.net/5/1855/2005/ doi: 10.5194/acp-5-1855-2005

Moussallam, Y., Rose-Koga, E., Koga, K., Médard, E., Bani, P., Devidal, J.-L., & Tari, D. (2019, 10). Fast ascent rate during the 2017–2018 Plinian eruption of Ambae (Aoba) volcano: a petrological investigation. *Contributions to Mineralogy and Petrology*, *174*, 90. doi: 10.1007/s00410-019-1625-z

Newman, P., Coy, L., & Pawson, S. (2019). *2018's Biggest Volcanic Eruption of Sulfur Dioxide.* Retrieved 2019-12-12, from https://acd-ext.gsfc.nasa.gov/Data_services/met/qbo/u_qbo_merra2_vs_p_00N.png

Punge, H. J., Konopka, P., Giorgetta, M. A., & Müller, R. (2009). Effects of the quasi-biennial oscillation on low-latitude transport in the stratosphere derived from trajectory calculations. *Journal of Geophysical Research: Atmospheres*, *114*(D3). Retrieved from https://agupubs.onlinelibrary.wiley.com/doi/abs/10.1029/2008JD010518 doi: 10.1029/2008JD010518

Ridley, D. A., Solomon, S., Barnes, J. E., Burlakov, V. D., Deshler, T., Dolgii, S. I., ... Vernier, J. P. (2014). Total volcanic stratospheric aerosol optical depths and implications for global climate change. *Geophysical Research Letters*, *41*(22), 7763-7769. Retrieved from https://agupubs.onlinelibrary.wiley.com/doi/abs/10.1002/2014GL061541 doi: 10.1002/2014GL061541

Robock, A., Adams, T., Moore, M., Oman, L., & Stenchikov, G. (2007). Southern Hemisphere atmospheric circulation effects of the 1991 Mount Pinatubo eruption. *Geophysical Research Letters*, *34*(23). Retrieved from https://agupubs.onlinelibrary.wiley.com/doi/abs/10.1029/2007GL031403 doi: 10.1029/2007GL031403

Sellitto, P., & Briole, P. (2015). On the radiative forcing of volcanic plumes: modelling the impact of mount etna in the mediterranean. *Annals of Geophysics*, *58*(0). Retrieved from https://www.annalsofgeophysics.eu/index.php/annals/article/view/6879 doi: 10.4401/ag-6879

Sellitto, P., di Sarra, A., Corradini, S., Boichu, M., Herbin, H., Dubuisson, P., ... Legras, B. (2016). Synergistic use of Lagrangian dispersion and radiative transfer modelling with satellite and surface remote sensing measurements for the investigation of volcanic plumes: the Mount Etna eruption of 25–27 October 2013. *Atmos Chem Phys*, *16*(11), 6841–6861. Retrieved from https://www.atmos-chem-phys.net/16/6841/2016/ doi: 10.5194/acp-16-6841-2016

Sellitto, P., Zanetel, C., di Sarra, A., Salerno, G., Tapparo, A., Meloni, D., ... Legras, B. (2017). The impact of Mount Etna sulfur emissions on the atmospheric composition and aerosol properties in the central Mediterranean: A statistical analysis over the period 2000–2013 based on observations and Lagrangian modelling. *Atmospheric Environment*, *148*, 77 - 88. Retrieved from http://www.sciencedirect.com/science/article/pii/S1352231016308391 doi: https://doi.org/10.1016/j.atmosenv.2016.10.032

Solomon, S., Daniel, J. S., Neely, R. R., Vernier, J.-P., Dutton, E. G., & Thomason, L. W. (2011). The Persistently Variable "Background" Stratospheric Aerosol Layer and Global Climate Change. *Science*, *333*(6044), 866–870. Retrieved from https://science.sciencemag.org/content/333/6044/866 doi: 10.1126/science.1206027

Stevenson, D. S., Johnson, C. E., Collins, W. J., & Derwent, R. G. (2003). The tropospheric sulphur cycle and the role of volcanic SO2. *Geological Society, London, Special Publications*, *213*(1), 295–305. Retrieved from https://sp.lyellcollection.org/content/213/1/295 doi: 10.1144/GSL.SP.2003.213.01.18

SunilKumar, S., Parameswaran, K., & Murthy, B. K. (2003). Lidar observations of cirrus cloud near the tropical tropopause: general features. *Atmospheric Research*, *66*(3), 203 - 227. Retrieved from http://www.sciencedirect.com/science/article/pii/S016980950200159X doi: https://doi.org/10.1016/S0169-8095(02)00159-X

Thomason, L. W., & Vernier, J.-P. (2013). Improved sage ii cloud/aerosol categorization and observations of the asian tropopause aerosol layer: 1989-2005. *Atmospheric Chemistry and Physics*, *13*(9), 4605–4616. Retrieved from https://www.atmos-chem-phys.net/13/4605/2013/ doi: 10.5194/acp-13-4605-2013

Trepte, C., & Hitchman, M. (1992). Tropical stratospheric circulation deduced from satellite aerosol data. *Nature*, *355*, 626–628. doi: https://doi.org/10.1038/355626a0

Uesawa, D. (2009). Clear Sky Radiance (CSR) product from MTSAT-1R. *Meteorological Satellite CenterTechnical Note*(52), 39-48.

van de Hulst, H. (1981). *Light Scattering by Small Particles*. Dover Publications. Retrieved from `https://books.google.fr/books?id=PlHfPMVAFRcC`

Vernier, J.-P., Fairlie, T. D., Deshler, T., Venkat Ratnam, M., Gadhavi, H., Kumar, B. S., ... Renard, J.-B. (2018). BATAL: The Balloon Measurement Campaigns of the Asian Tropopause Aerosol Layer. *Bulletin of the American Meteorological Society*, *99*(5), 955-973. Retrieved from `https://doi.org/10.1175/BAMS-D-17-0014.1` doi: 10.1175/BAMS-D-17-0014.1

Vernier, J.-P., Fairlie, T. D., Natarajan, M., Wienhold, F. G., Bian, J., Martinsson, B. G., ... Bedka, K. M. (2015). Increase in upper tropospheric and lower stratospheric aerosol levels and its potential connection with Asian pollution. *J Geophys Res*, *120*(4), 1608-1619. Retrieved from `https://agupubs.onlinelibrary.wiley.com/doi/abs/10.1002/2014JD022372` doi: 10.1002/2014JD022372

Vernier, J.-P., Thomason, L. W., & Kar, J. (2011). CALIPSO detection of an Asian tropopause aerosol layer. *Geophys Res Lett*, *38*(7). Retrieved from `https://agupubs.onlinelibrary.wiley.com/doi/abs/10.1029/2010GL046614` doi: 10.1029/2010GL046614

Winker, D. M., Hostetler, C., Vaughan, M., & Omar, A. (2006). CALIOP Algorithm Theoretical Basis Document Part 1: CALIOP Instrument, and Algorithms Overview. *CALIPSO*, *2*(PC-SCI-202 Part 1), 1-29. Retrieved from `https://www-calipso.larc.nasa.gov/resources/pdfs/PC-SCI-202.Part1_v2-Overview.pdf`

Winker, D. M., Pelon, J., Coakley, J. A., Ackerman, S. A., Charlson, R. J., Colarco, P. R., ... Wielicki, B. A. (2010). The CALIPSO Mission. *Bulletin of the American Meteorological Society*, *91*(9), 1211-1230. Retrieved from `https://doi.org/10.1175/2010BAMS3009.1` doi: 10.1175/2010BAMS3009.1

Woods, A., & Self, S. (1992). Thermal disequilibrium at the top of volcanic clouds and its effect on estimates of the column height. *Nature*(355), 628–630. doi: doi:10.1038/355628a0

Yu, P., Toon, O. B., Bardeen, C. G., Zhu, Y., Rosenlof, K. H., Portmann, R. W., ... Robock, A. (2019). Black carbon lofts wildfire smoke high into the stratosphere to form a persistent plume. *Science*, *365*(6453), 587–590. Retrieved from `https://science.sciencemag.org/content/365/6453/587` doi: 10.1126/science.aax1748